A NON OVERLAPPING CAMERA NETWORK: CALIBRATION AND APPLICATION TOWARDS LANE DEPARTURE WARNING

Amol Borkar

Georgia Institute of Technology
Atlanta, GA, USA
amol@gatech.edu

Monson Hayes

Chung Ang University
Seoul, Korea
monson.hayes@gatech.edu

Mark T. Smith

Kungliga Tekniska Högskolan
Stockholm, Sweden
msmith@kth.se

ABSTRACT

In this paper, we present a new multi camera approach to Lane Departure Warning (LDW). First, a perspective removal transformation is applied to the camera captured images to convert them into bird's-eye view images. Then, the position of the two cameras relative to a reference point is accurately determined using a new calibration technique. Lane detection is performed on the front and rear camera images who results are combined using data fusion. Finally, LDW is implemented by determining the distance between the vehicle and adjacent lane boundaries. The proposed system was tested on real world driving videos and shows good results when compared to ground truth.

Index Terms— Lane departure warning; multi camera calibration; non-overlapping camera networks; data fusion.

1. INTRODUCTION

Driver Assistance (DA) systems are common accessory in today's passenger and commercial vehicles. DA systems as the name suggests are systems that provide aid or feedback to the driver of a vehicle. One example of such a system is Lane Departure Warning (LDW). LDW is a safety feature that informs the driver if the vehicle appears to change lanes unless certain conditions are met e.g. turn indicator is on. The hardware often consists of a single camera which acquires images out of the front windshield that are analyzed to determine if the vehicle is within a certain distance of a lane boundary.

Although LDW has been in research for many years, it has only been recently that LDW systems have started appearing in luxury cars and as after market products. Variations of the Time to Lane Crossing (TLC) are some one of the most popular techniques used for LDW [1, 2, 3, 4, 5]. In TLC, the future position of the vehicle is estimated based on the steering angle and by extrapolating detected lane positions, then the driver is warned if a lane crossing is predicted. The lane detection component of LDW often produces noisy results; consequently, the extrapolated estimates may not accurately represent future lane positions leading to false signaling. Other LDW techniques involve determining the angles or orientations of detected lane boundaries to hypothesize a distance metric [6, 7, 8]. Actual distance to the adjacent boundaries is not computed. In this paper, we compute the immediate distance between the vehicle and adjacent boundaries using known camera geometries. In addition, we add a second camera that looks out of the rear windshield. This provides redundant lane boundary position information which is used in data fusion.

Since we are combining data from multiple cameras, calibration is important. Calibration for stereo and n-camera setups is often performed using variations of standard test patterns like checkerboard to establish a baseline [9]. However, a caveat of these techniques is that each camera needs to be able to see the same checkerboard i.e. the cameras need to have some overlap in their fields of view. Since our cameras are facing in opposite directions, the checkerboard methods are ineffective. Referring to non-overlapping camera networks, work has been conducted in [10, 11, 12]. The method shown in [10, 11] uses a planar mirror while [12] uses a moving rig to calibrate each camera. However, the rig movement appears arbitrary which can severely affect the estimates of camera positions. A similar experiment with a multi camera setup for vehicular applications has been shown in [13]; however, there is not much detail on camera placement relative to each other and data merging for lane detection or LDW. For our work, we have devised a new yet simple calibration technique that allows to accurately determine the position of the two cameras in the vehicle.

This paper is organized as follows: subsequent to the introduction, the details of camera calibration are described. The importance of establishing a common co-ordinate system is also explained. The procedure for combining lane detection results from the front and rear cameras is described. Finally, LDW is completed by explaining the technique used to measure the distance to lane boundaries. The proposed approach was compared to a single camera LDW system as well as ground truth and showed good results when tested on real world driving videos.

2. CAMERA CALIBRATION

2.1. Perspective Removal

The camera acquired images undergo a geometric transformation known as Inverse Perspective Mapping (IPM) to remove the effects of perspective from the image [14]. With IPM, the captured images are transformed to appear as a birds-eye view in which lane markers appear as nearly parallel lines of constant thickness. An example of a camera acquired image and IPM transformed image are shown in Fig. 1. The mapping from world co-ordinates $(x, y, z = 0)$ to image co-ordinates (r, c) is given as

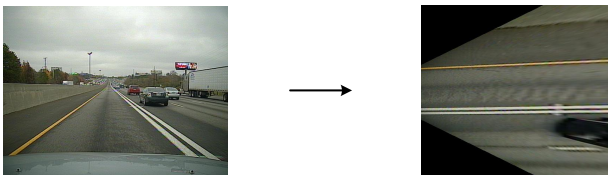

Fig. 1: The camera image on the left and transformed image on the right.

$$r(x) = \frac{M-1}{2}\left(1 + \frac{h - x' \cdot \tan\theta_o}{h \cdot \tan\theta_o + x'} \cdot \cot\alpha_v\right) + 1 \quad (1)$$

$$c(x,y) = \frac{N-1}{2}\left(1 - \frac{y'}{h \cdot \sin\theta_o + x' \cdot \cos\theta_o} \cdot \cot\alpha_u\right) + 1 \quad (2)$$

where h is the height of the camera, θ_o is the pitch, α_u is the horizontal field of view, α_v is the vertical field of view, γ is the yaw, and $(M \times N)$ is the size of the camera image. Furthermore

$$\begin{bmatrix} x' \\ y' \end{bmatrix} = \begin{bmatrix} \cos\gamma & -\sin\gamma \\ \sin\gamma & \cos\gamma \end{bmatrix} \begin{bmatrix} x \\ y \end{bmatrix} \quad (3)$$

provides the yaw correction by rotating the world co-ordinates about the optical center of the camera. The mapping shown above allows for different horizontal and vertical field of view angles where as the [14] assumes them to be equal.

2.2. Calibration

In camera calibration, a reference origin needs to be specified. This location is chosen as the center of the vehicle as shown in Fig. 2 and denoted as $\mathbf{P_o} = \begin{bmatrix} 0 & 0 & 0 \end{bmatrix}^T$. The reference co-ordinate system is shown on the right in Fig. 2. The positions of the front and rear cameras relative to $\mathbf{P_o}$ are then determined. These position are denoted as $\mathbf{P_f}$ for the front camera and $\mathbf{P_r}$ for the rear camera. Since $\mathbf{P_r}$ looks out of the back window, its IPM image is rotated $180°$. Small measurement errors in $\mathbf{P_f}$ and $\mathbf{P_r}$ could lead to critical errors during data fusion used later; therefore, the accuracy of these

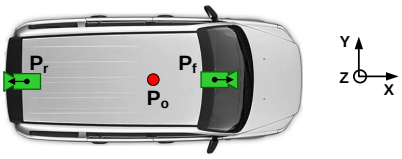

Fig. 2: Position of the origin and two cameras.

measurements is verified by comparing to reference data subject to certain constraints. The reference data is made up of images captured while driving at a constant speed near the middle of a straight road where the distance between adjacent lane boundaries is constant and uniform. Both cameras undergo basic calibration to determine yaw (γ) and pitch (θ_o) which prevents the lane boundaries from appearing skewed or tilted in the IPM image. Therefore, the cameras are now $180°$ opposed and facing in opposite directions along the X-axis of the reference co-ordinate system shown in Fig. 2. Sample front and rear camera images are shown in Fig. 3. Correctness

(a) Front camera image. (b) Rear camera image.

Fig. 3: Sample camera images.

is assumed in the measured X and Y co-ordinates of $\mathbf{P_f}$. The techniques described below accurately determine the height of $\mathbf{P_f}$ as well as the translation of $\mathbf{P_r}$ relative to $\mathbf{P_o}$.

2.2.1. *Height verification*

We combine Eq. (1) and (2) to determine the mapping of a pixel from the camera to world co-ordinates as

$$Y(r,c) = h\left(\frac{[1 - 2(\frac{c-1}{N-1})]\tan\alpha_u}{\sin\theta_o - [1 - 2(\frac{r-1}{M-1})]\tan\alpha_v \cos\theta_o}\right) \quad (4)$$

We choose two points (r, c_1) and (r, c_2) on adjacent lane boundaries in the camera image and find their corresponding mappings to the IPM domain as $Y(r, c_1)$ and $Y(r, c_2)$ respectively as shown in Fig. 4. Since it not possible to park on the highway and physically measure the distance between adjacent lane boundaries, we refer to Federal Highway Administrations (FHA) handbook regarding specification for painted markings [15] where it is stated that the distance between lane boundaries on highways is on average 12ft. Using this information, we can set

$$Y(r,c_1) - Y(r,c_2) = \Delta Y = 12 \text{ feet} \quad (5)$$

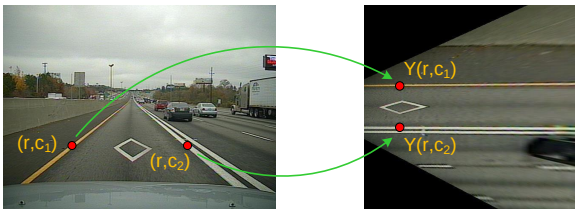

Fig. 4: Mapping points from the camera image to IPM image.

Hence, we substitute Eq. (4) in Eq. (5) and solve for h as

$$h = \Delta Y \left(\frac{\sin\theta_o - [1 - 2(\frac{r-1}{M-1})] \tan\alpha_v \cos\theta_o}{2[\frac{c_2 - c_1}{N-1}] \tan\alpha_u} \right) \quad (6)$$

Similarly, we can repeat this procedure to determine the height of the rear camera.

2.2.2. *Offset between cameras*

There will be a noticeable offset between the lane markings when observed in each IPM image if the two cameras are not aligned properly. This can be seen in Fig. 5 by placing the two IPM images side by side. Since the $\mathbf{P_f}$ is assumed to be inline with the origin, the rear camera is translated along the Y-axis till the lane markings line up correctly. The translation in the IPM image is scaled to world units to determine the actual offset between the two cameras.

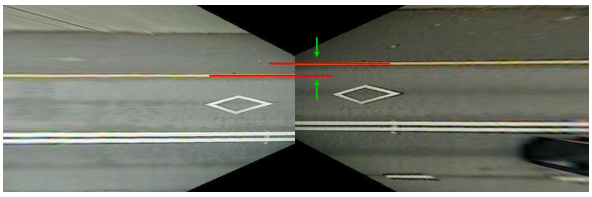

Fig. 5: Error in camera camera alignment. This results in lane markings being offset from one view to the other.

2.2.3. *Distance between cameras*

To determine the distance between the cameras, we first need to find objects with corners in each IPM image. Since the diamond painted in middle of the high occupancy vehicle (HOV) lane has noticeable corners, it satisfies our requirement. This is shown in Fig. 6. Knowing the commuting speed of the vehicle and the time delay since the diamond from the front camera IPM image reappears in the rear camera IPM image, the total covered distance can be computed as

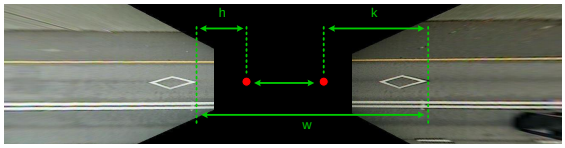

Fig. 6: Determining the distance between the cameras.

$$w = \text{Speed} \times \text{Time Delay} \quad (7)$$

By setting $(x = 0, y = 0)$ in Eq. (3), the optical center of each camera relative to its IPM image can be determined and is illustrated by the red dots in Fig. 6. Since the lens used in this implementation has a focal length of 5mm, it to safe to assume that the optical center is analogous to the camera position. As a result, it is possible to determine both distances h and k between specific points on the diamond and the camera itself. Consequently, the distance between the cameras can estimated as

$$\text{Distance between cameras} = w - (h + k) \quad (8)$$

3. LANE DETECTION

Lane detection is performed using the technique presented in [16] on both forward and rear camera views. Following IPM, the transformed image is converted from RGB to YCbCr to aid in color segmentation. Then, the images are cross-correlated with a collection of predefined templates to find candidate lane regions. These regions then undergo connected components analysis, morphological operations, and elliptical projections to approximate positions of the lane markers. The implementation of the Kalman filter enables tracking lane markers on curved roads while RANSAC helps improve estimates by eliminating outliers [16].

4. COMMON CO-ORDINATE SYSTEM

In a standalone IPM image, the optical center e.g. $\mathbf{P_f}$ is at the origin. Each pixel in the IPM image has a certain (x, y) co-ordinate relative its optical center. This approach is acceptable when dealing with a single camera; however, when dealing with multiple cameras, a common co-ordinate system needs to be established.

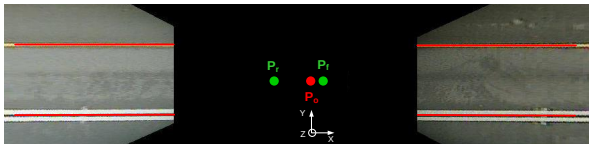

Fig. 7: Position of the origin and two cameras.

In our implementation, $\mathbf{P_o}$ is chosen as the origin of this space and shown as a red dot in Fig. 7 with the reference co-ordinate orientation shown near the bottom. The two green dots in Fig. 7 represent $\mathbf{P_f}$ and $\mathbf{P_r}$. Next, a transformation $\mathbf{T_f}$ that maps the only (x, y) co-ordinates of $\mathbf{P_o}$ to $\mathbf{P_f}$ is determined. $\mathbf{T_f}$ is only a translation as rotation is implied in

the creation of the birds-eye view image. This transformation when applied to the IPM image maps the (x, y) co-ordinates of every pixel to a location in a co-ordinate system that is relative to $\mathbf{P_o}$. Consequently, the lane boundaries detected in the front camera IPM image are also mapped to the space described by (x, y) co-ordinates relative to $\mathbf{P_o}$. A transformation mapping $\mathbf{P_o}$ to $\mathbf{P_r}$ is similarly computed and used to relocate the rear camera IPM pixels to the co-ordinate space relative to $\mathbf{P_o}$.

The importance of setting up a common coordinate system is that the lane boundary locations detected in the front and rear IPM images are now described relative to $\mathbf{P_o}$ rather than their respective optical centers.

5. LANE DEPARTURE WARNING

Upon completing the front and rear lane detections, data fusion in the form of a parametric cubic Hermite spline connects the detected lane boundaries from each view. Using four points as shown in Fig. 8, the locations of lane boundaries outside the camera views can be estimated. An analytical representation of the spline is given in below

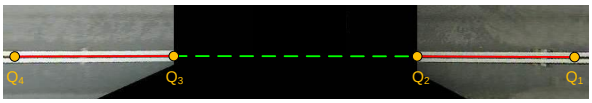

Fig. 8: Estimated boundary shown as dotted green line using Catmull-Rom spline.

$$\mathbf{Q}(t) = \begin{bmatrix} 1 & t & t^2 & t^3 \end{bmatrix} \begin{bmatrix} 0 & 1 & 0 & 0 \\ -\tau & 0 & \tau & 0 \\ 2\tau & \tau-3 & 3-2\tau & -\tau \\ -\tau & 2-\tau & \tau-2 & \tau \end{bmatrix} \begin{bmatrix} \mathbf{Q}_1 \\ \mathbf{Q}_2 \\ \mathbf{Q}_3 \\ \mathbf{Q}_4 \end{bmatrix} \quad (9)$$

where τ provides the tension for the curve and is assigned a value between $[0, 1]$. Since, we are using a Catmull-Rom spline to produce a smooth curve, τ is set to 0.5 [17].

Upon completing camera calibration and data fusion, the following is known:

1. Center of the vehicle.
2. Dimensions of a reference vehicle.
3. Location of lane boundaries.

Using the available information, the distance to the lane boundary (in feet) on either side of the vehicle can be calculated as:

$$\text{Distance to marking} = |\text{LB}_{x=0} - \text{sign}[\text{LB}_{x=0}](\frac{\text{Width}}{2})| \text{ feet} \quad (10)$$

where $\text{LB}_{x=0}$ is simply the y-value of the estimated lane boundary from Eq. (9) evaluated at x=0. The green bounding box in Fig. 9 depicts the dimensions of the reference vehicle in the common co-ordinate space with $\mathbf{P_o}$ as the red dot. Using Eq. (10), LDW can be systematically performed by warning the driver if the vehicle is within a minimum distance from a lane boundary.

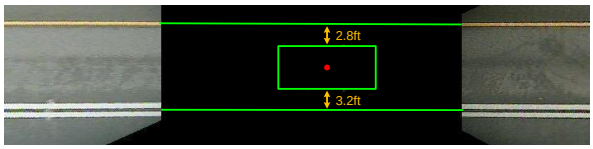

Fig. 9: Distance to lane boundaries on either side.

To assist the driver, a visualization is created by overlaying a scaled image of a reference vehicle with estimated lane boundaries on either side as shown in Fig. 10 .

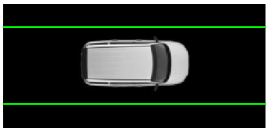

Fig. 10: Visualization of the vehicle and estimated lane boundaries.

6. RESULTS

Two time-synchronized NTSC cameras were used in acquiring video streams for testing. The streams were captured while driving on roadways in and around Atlanta, GA, USA. Several minutes worth of videos were used in testing. The rear camera was inoperable at night without artificial illumination; hence, testing was restricted to day time only. Additionally, testing was was conducted only on highway footage as most commercial LDW systems operate above 45mph [18, 19].

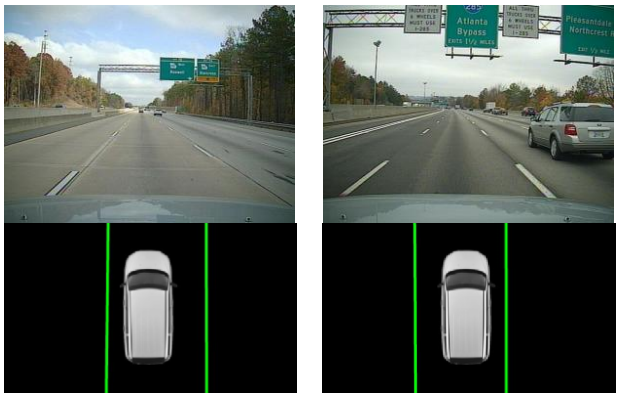

(a) (b)

Fig. 11: Front camera image and estimated position of the vehicle within the lane.

In Fig. 11, a few examples of the images captured by the front camera with an overhead visualization estimating the position of the vehicle within a lane are shown. Fig. 12 shows an example of the vehicle approaching very close to a lane boundary over the duration of a clip. When the vehicle is within 0.75ft of a lane boundary, a warning is signaled. To prevent flickering near the threshold, hysteresis is used whereby the vehicle needs to travel more than 1ft away from the lane boundary for the warning to be disabled. Fig. 12c shows a plot of the estimated distance between the right lane boundary and vehicle over the duration of the video. The plot also shows a comparison between the multi camera approach, single camera approach and ground truth. To estimate distance using a single camera, we refer back to Fig. 8 and evaluate the line formed by $\mathbf{Q}_1$ and $\mathbf{Q}_2$ at x=0. A straight line model is less affected by noise in lane detection results; hence, it is used for extrapolation. Ground truth estimates are produced using a Catmull-Rom spline [17] between the ground truth lane boundary locations in the front and rear camera images. In Fig. 12c, it can be observed that the estimates of the multi camera approach are often very close to the ground truth. The single camera approach fares well on straight roads but face difficult when encountered with a curve. Fig. 12d provides a visual comparison between the ground truth, single camera and multi camera approach when the vehicle encounters a turn in the test clip.

In a single camera setup, estimating distances to the lane boundaries is an extrapolation problem. However, in the proposed approach, estimating the distances is an interpolation problem which appears to be more accurate and affective.

Errors in lane detection reflect directly on the lane boundary estimates as these estimates are calculated based on the findings of the front and rear lane detectors. A few instances of incorrect lane detections shown in Fig. 13 resulted in incorrect estimates of the distances to the lane boundaries. In addition, when an incomplete lane detection occurs i.e. only one boundary is detected in either front or rear camera images, the estimates around the vehicle cannot be determined. This is shown in Fig. 13b.

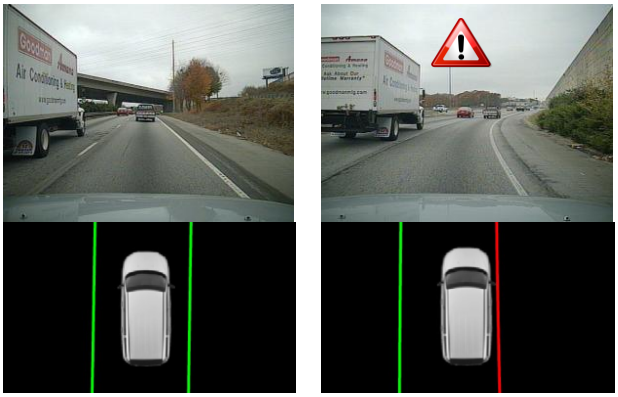

(a) Frame 73. (b) Frame 289.

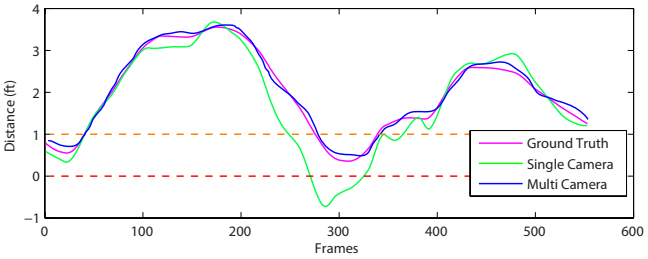

(c) Distance between vehicle and right lane marker.

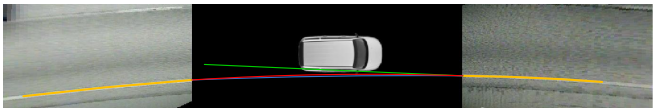

(d) Comparison between ground truth (red), single camera (green) and multi camera (blue) approach. Detected lane markings are shown in orange.

Fig. 12: An example of Lane Departure Warning (LDW).

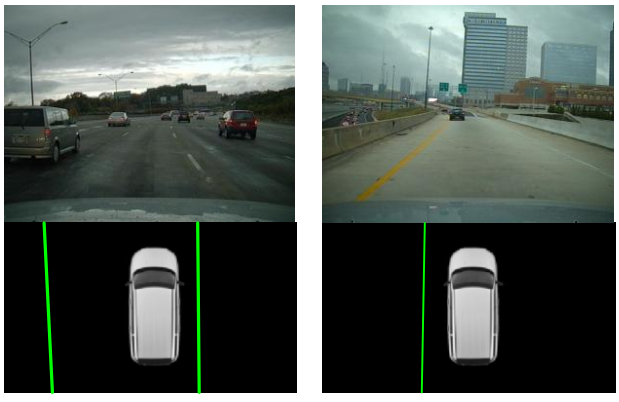

(a) (b)

Fig. 13: A few examples where the multi-camera approach faces difficulty.

7. CONCLUSION

Presented in this paper is a novel approach to Lane Departure Warning (LDW) using multiple cameras. First, the captured images undergo a perspective removal transform to produce a bird's-eye view image. Then, the positions of two cameras accurately determined using calibration. Following lane detection, data fusion is used to connect the detected lane boundaries from one camera view to the other. By determining the distance between the vehicle and lane boundaries, an LDW system is realized. The proposed setup showed good results when tested with real world driving videos. The multi camera approach also produced estimates close to the ground truth on both straight and curved roads in the test data while the single camera approach faced difficulty on the curved roads.

8. FUTURE WORK

The presented work is part of on going research. Handling situations when an incomplete lane detection occur needs to be investigated. Kalman or particle filters will be used to track $LB_{x=0}$ on either side of the vehicle. Additional tests with complex scenarios will be conducted. Illumination hardware to enable night time multi camera usage will be purchased.

9. REFERENCES

[1] D.J. LeBlanc, G.E. Johnson, P.J.T. Venhovens, G. Gerber, R. DeSonia, R.D. Ervin, C.F. Lin, A.G. Ulsoy, and T.E. Pilutti, "CAPC: A road-departure prevention system," *Control Systems Magazine, IEEE*, vol. 16, no. 6, pp. 61–71, 1996.

[2] W. Kwon, J.W. Lee, D. Shin, K. Roh, D.Y. Kim, and S. Lee, "Experiments on decision making strategies for a lane departure warning system," in *Robotics and Automation, 1999. Proceedings. 1999 IEEE International Conference on*. IEEE, 1999, vol. 4, pp. 2596–2601.

[3] S.Y. Kim and S.Y. Oh, "A driver adaptive lane departure warning system based on image processing and a fuzzy evolutionary technique," in *Intelligent Vehicles Symposium, 2003. Proceedings. IEEE*. IEEE, pp. 361–365.

[4] X. Dai, A. Kummert, S.B. Park, and D. Neisius, "A warning algorithm for Lane Departure Warning system," in *Intelligent Vehicles Symposium, 2009 IEEE*. IEEE, pp. 431–435.

[5] X. An, M. Wu, and H. He, "A novel approach to provide lane departure warning using only one forward-looking camera," in *Collaborative Technologies and Systems, 2006. CTS 2006. International Symposium on*. 2006, IEEE Computer Society.

[6] P.Y. Hsiao, C.W. Yeh, S.S. Huang, and L.C. Fu, "A portable vision-based real-time lane departure warning system: day and night," *Vehicular Technology, IEEE Transactions on*, vol. 58, no. 4, pp. 2089–2094, 2009.

[7] Qing Lin, Youngjoon Han, and Hernsoo Hahn, "Real-time Lane Detection Based on Extended Edge-linking Algorithm," in *Computer Research and Development, 2010 Second International Conference on*, 2010, pp. 725–730.

[8] Yu-Chi Leng and Chieh-Li Chen, "Vision-based lane departure detection system in urban traffic scenes," in *Control Automation Robotics Vision (ICARCV), 2010 11th International Conference on*, 2010, pp. 1875–1880.

[9] Richard Hartley and Andrew Zisserman, *Multiple View Geometry in Computer Vision*, Cambridge University Press, 2 edition, Apr. 2004.

[10] P. Lébraly, C. Deymier, O. Ait-Aider, E. Royer, and M. Dhome, "Flexible extrinsic calibration of non-overlapping cameras using a planar mirror: Application to vision-based robotics," in *Intelligent Robots and Systems (IROS), 2010 IEEE/RSJ International Conference on*. IEEE, 2010, pp. 5640–5647.

[11] R.K. Kumar, A. Ilie, J.M. Frahm, and M. Pollefeys, "Simple calibration of non-overlapping cameras with a mirror," in *Computer Vision and Pattern Recognition, 2008. CVPR 2008. IEEE Conference on*. 2008, IEEE.

[12] F. Pagel, "Calibration of non-overlapping cameras in vehicles," in *Intelligent Vehicles Symposium (IV), 2010 IEEE*. IEEE, pp. 1178–1183.

[13] S.S. Ieng, J. Vrignon, D. Gruyer, and D. Aubert, "A new multi-lanes detection using multi-camera for robust vehicle location," in *Intelligent Vehicles Symposium, 2005. Proceedings. IEEE*. IEEE, 2005, pp. 700–705.

[14] M. Bertozzi and A. Broggi, "GOLD: a parallel real-time stereo vision system for generic obstacle and lane detection," *IEEE Transactions on Image Processing*, vol. 7, no. 1, pp. 62–81, 1998.

[15] Federal Highway Administration, "Manual Uniform Traffic Control Devices," Nov. 2009.

[16] A. Borkar, M. Hayes, and M. Smith, " A Template Matching And Ellipse Modeling Approach To Detecting Lane Markers," in *2010 Advanced Concepts for Intelligent Vision Systems (ACIVS 2010)*, 2010, pp. 179–190.

[17] E. Catmull and R. Rom, "A class of local interpolating splines," *Computer Aided Geometric Design*, vol. 74, pp. 317–326, 1974.

[18] Infiniti USA, "2012 Infiniti M Specs & Options," 2011.

[19] Mercedes-Benz USA, "2011 Mercedes-Benz S550 Specs," 2011.